Earth and Space Science

RESEARCH ARTICLE
10.1029/2023EA002879

Key Points:

- The extraordinary dust episode over the Balkan region was simulated with the WRF-Chem model
- The dried Aral Sea was identified as the main source, but the dust plume from the Sahara was also present
- Chemical and morphological analysis of the PM_{10} sample shows that the dust originated from the Sahara Desert

Supporting Information:

Supporting Information may be found in the online version of this article.

Correspondence to:

B. Mifka,
boris.mifka@phy.uniri.hr

Citation:

Mifka, B., Telišman Prtenjak, M., Kavre Piltaver, I., Mekterović, D., Kuzmić, J., Marciuš, M., & Ciglenečki, I. (2023). Intense desert dust event in the northern Adriatic (March 2020); insights from the numerical model application and chemical characterization results. *Earth and Space Science*, *10*, e2023EA002879. https://doi.org/10.1029/2023EA002879

Received 15 FEB 2023
Accepted 22 MAY 2023

Author Contributions:

Conceptualization: Boris Mifka, Maja Telišman Prtenjak, Irena Ciglenečki
Data curation: Boris Mifka, Ivna Kavre Piltaver
Formal analysis: Maja Telišman Prtenjak, Ivna Kavre Piltaver, Darko Mekterović, Josipa Kuzmić, Marijan Marciuš, Irena Ciglenečki
Funding acquisition: Maja Telišman Prtenjak, Darko Mekterović, Irena Ciglenečki

Intense Desert Dust Event in the Northern Adriatic (March 2020); Insights From the Numerical Model Application and Chemical Characterization Results

Boris Mifka[1], Maja Telišman Prtenjak[2], Ivna Kavre Piltaver[1,3], Darko Mekterović[1], Josipa Kuzmić[4], Marijan Marciuš[5], and Irena Ciglenečki[6]

[1]Faculty of Physics, University of Rijeka, Rijeka, Croatia, [2]Department of Geophysics, Faculty of Science, University of Zagreb, Zagreb, Croatia, [3]Centre for Micro- and Nanosciences and Technologies, University of Rijeka, Rijeka, Croatia, [4]Croatian Meteorological and Hydrological Service, Zagreb, Croatia, [5]Division of Materials Chemistry, Ruđer Bošković Institute, Zagreb, Croatia, [6]Laboratory for Physical Oceanography and Chemistry of Aquatic Systems, Division for Marine and Environmental Research, Ruđer Bošković Institute, Zagreb, Croatia

Abstract The uncharacteristically extreme outbreak of particulate matter took place over the Balkan region from 27 to 30 March 2020. Observations at air quality stations in Croatia recorded hourly PM_{10} concentrations up to 412 μgm^{-3}. The meteorological analysis shows that the increase in PM_{10} concentrations was primarily due to the advection of dust from the deserts east of the Caspian Sea. The anticyclone north of Croatia and the cyclone over Anatolia formed a strong pressure gradient driving transport from the east. Both back trajectories and satellite products pointed to the dry Aral Sea as the main source of dust. A dust plume influenced the PM_{10} increase observed in Croatia, starting at the easternmost air quality stations. The modeling study shows that the vertical extent of the dust plume was up to ∼2 km. However, the chemical and morphological (scanning electron microscope analysis) composition of PM_{10} at the sites in the northeastern Adriatic Sea showed mainly the presence of Saharan dust. Prior to the advection of the Asian dust, the transport of Saharan dust, driven by Sharav cyclone, was observed in the PM_{10} values at several stations in the Adriatic Sea and on the Croatian mainland on 26 March 2020. Modeling results showed that the Saharan dust transport occurred at altitudes below ∼8 km. The mixing of the Asian and Saharan dust plumes over the Balkans was favored by the subsidence due to anticyclonic high-pressure conditions and is the most likely explanation for the observed PM chemical and morphological results.

Plain Language Summary The event of extreme air pollution in Croatia occurred at the end of March 2020. Exceptionally high aerosol concentrations were observed at several air quality stations. The outbreak was studied using a numerical chemical transport model. Chemical analysis was also performed for the aerosol sample and the sample was viewed with an electronic microscope. The analysis revealed that the composition of the aerosol was due to desert dust transported by air masses from the deserts east of the Caspian Sea and the Sahara Desert.

1. Introduction

Particulate matter from suspended mineral dust is one of the most abundant aerosols and is a growing climate change and air quality concern directly related to public health. Dust aerosols have an impact on radiation (Li & Sokolik, 2018) and cloud microphysics (Tsarpalis et al., 2020). When deposited in the ocean (Richon et al., 2018) or on land (Kylander et al., 2018), they provide micronutrients to ecosystems (Mifka et al., 2022b).

The general problem with estimating dust emissions is the lack of measurements over the vast desert areas, and dust emissions are obtained from models that are highly variable in their estimates. This affects the simulated dust concentration in the air, especially deposition, which is rarely measured (Vincent et al., 2016). According to the study by Huneeus et al. (2011), modeled global dust emissions range from 514 to 4,313 Tg yr^{-1}, while deposition ranges from 676 to 4,359 Tg yr^{-1}. The more advanced approach to emission estimates is in the form of gridded reanalysis data, where modeled values are improved by assimilating optical properties observed with satellites (Buchard et al., 2017). The recent study by Kok et al. (2021a), using inverse modeling for the period 2004–2008, found even higher global dust emissions (up to ∼5,000 Tg yr^{-1}) compared to most models. This is due to the

Investigation: Boris Mifka, Maja Telišman Prtenjak, Ivna Kavre Piltaver, Darko Mekterović, Josipa Kuzmić, Marijan Marciuš, Irena Ciglenečki
Methodology: Maja Telišman Prtenjak
Resources: Boris Mifka, Ivna Kavre Piltaver, Irena Ciglenečki
Supervision: Maja Telišman Prtenjak, Darko Mekterović
Validation: Boris Mifka, Maja Telišman Prtenjak, Irena Ciglenečki
Visualization: Boris Mifka, Ivna Kavre Piltaver
Writing – original draft: Boris Mifka, Maja Telišman Prtenjak, Ivna Kavre Piltaver, Josipa Kuzmić, Irena Ciglenečki
Writing – review & editing: Boris Mifka, Maja Telišman Prtenjak, Ivna Kavre Piltaver, Darko Mekterović, Josipa Kuzmić, Marijan Marciuš, Irena Ciglenečki

greater emission of dust particles up to 20 μm in diameter (PM_{20}), which is underestimated in the models (Kok et al., 2021a).

The Sahara is the main global source of dust, accounting for 46% of global natural dust emissions (Kok et al., 2021b). About 100 Tg yr^{-1} of dust from North Africa is transported toward Europe (Schepanski et al., 2016; Shao et al., 2011), and several studies (e.g., Israelevich et al., 2012; Moulin et al., 1998; Shao et al., 2011; Varga, 2020) confirm that the Sahara is the main source of dust over the Mediterranean Sea. Advection toward Europe has an annual cycle that depends on global circulation and synoptic conditions, while dust emission itself depends strongly on surface winds in the atmospheric boundary layer (Engelstaedter et al., 2006). The northerly (N) and northeasterly (NE) winds converge with the moist maritime winds at 5–10°N in winter. This process controls the intertropical convergence zone (ITCZ), which shifts northward over the desert regions in spring and summer. The wind convergence favors the development of deep convection leading to dust storms Haboobs (Pantillon et al., 2016). The other dominant process (Heinold et al., 2013) of dust emission is the morning collapse of the nocturnal low-level jet (NLLJ).

Dust transport over the Mediterranean Sea depends strongly on Mediterranean cyclones (e.g., Fiedler et al., 2014; Flaounas et al., 2022; Schepanski et al., 2016). Despite the sporadic nature of the outbreaks, the highest dust levels in the eastern and central Mediterranean region occur in March and April (Barnaba & Gobbi, 2004; Mifka et al., 2022b; Moulin et al., 1998). In spring, the strong baroclinic gradients at the surface between the cold sea surface and the warm North African soil, together with the lee effect of the Atlas Mountains, lead to the development of Sharav cyclones that move rapidly eastward at a speed of about 10 ms^{-1} and cross the Mediterranean Sea between Libya and Egypt (Alpert & Ziv, 1989). The dust uplift is associated with the intense warm front and can reach heights of 500 hPa and above. The meridional component of the wind dominates the zonal one (Varga, 2020), resulting in intense dust transport toward the central Mediterranean, including the Adriatic Sea (Mifka et al., 2022b). Studies on dust case modeling in the Mediterranean are becoming more frequent, leading to operational dust forecasts of global and regional nature (Benedetti et al., 2014).

In contrast to these findings and practice, an unusual and intense dust outbreak occurred over southeastern Europe in March 2020, transporting dust from the deserts eastward to the Caspian Sea. There is not much evidence in the literature of dust advection from Asia to this part of Europe, and this pathway was not found in the climatological study for the period 2005–2013 (Ge et al., 2016). This study showed that dust is transported from the Aral Sea to the wider Caspian Sea area in every season. However, advection from the Aralkum Desert to Lithuania and Belarus has been documented (Goudie & Middleton, 2006). The Aral Sea is a vast terminal lake that has been dried up due to irrigation purposes, and its area has been reduced by 74% since the 1960s (Micklin, 2007), resulting in negative ecological feedbacks, climate change (Sharma et al., 2018), and severe health problems (Wæhler & Dietrichs, 2017) in the surrounding areas. The area became vulnerable to dust storms, with a significant trend in the frequency of dust storms in the last two decades of the last century. During the period 1936–1960, there were 35 days of dust storms per year (DS/yr), increasing to 65 days of DS/yr during the period 1980–2000 (Indoitu et al., 2012). This number is comparable to major source regions for dust storms such as the Sahel-Sudan region, where dust storms occur on up to 80 days of DS/yr (Goudie & Middleton, 2006). The Ozone Monitoring Instrument Aerosol Index (OMI AI) over the Aral Sea has also shown a rapidly increasing trend since 2005 (Ge et al., 2016).

This particular event took place in late March 2020 (i.e., 26–30 March 2020) and has already attracted the attention of the scientific community. Among the first studies to analyze this phenomenon were those by Strelec Mahović et al. (2020) and Tositti et al. (2022). Both studies were based on the analysis of (in situ and remote) measurements, reanalyses, and backward HYSPLIT trajectories. Strelec Mahović et al. (2020) analyzed in advance the observed PM_{10} concentrations at stations in the Pannonian part of Croatia. The highest values of up to ∼400 μg m^{-3} (on 27 March 2020 at 14 UTC) were measured in the mentioned case in Zagreb (Croatia), which was the most polluted city in Europe at that time. Other stations in the continental part of Croatia as well as in neighboring countries of the Balkan Peninsula also showed extremely poor air quality. Backward trajectories and satellite images (Meteosat-8 Dust RGB) pointed to the Aral region as the area from which dust transport occurred. It should be mentioned that the Adriatic region was not considered in this analysis. The second study by Tositti et al. (2022) is based on a detailed investigation of the event in northern Italy with an analysis of in situ and remote measurements in the area extending from Trieste to Bologna and Mount Cimone (Figure 1b). The authors used optical particle counter (OPC) data and, in combination

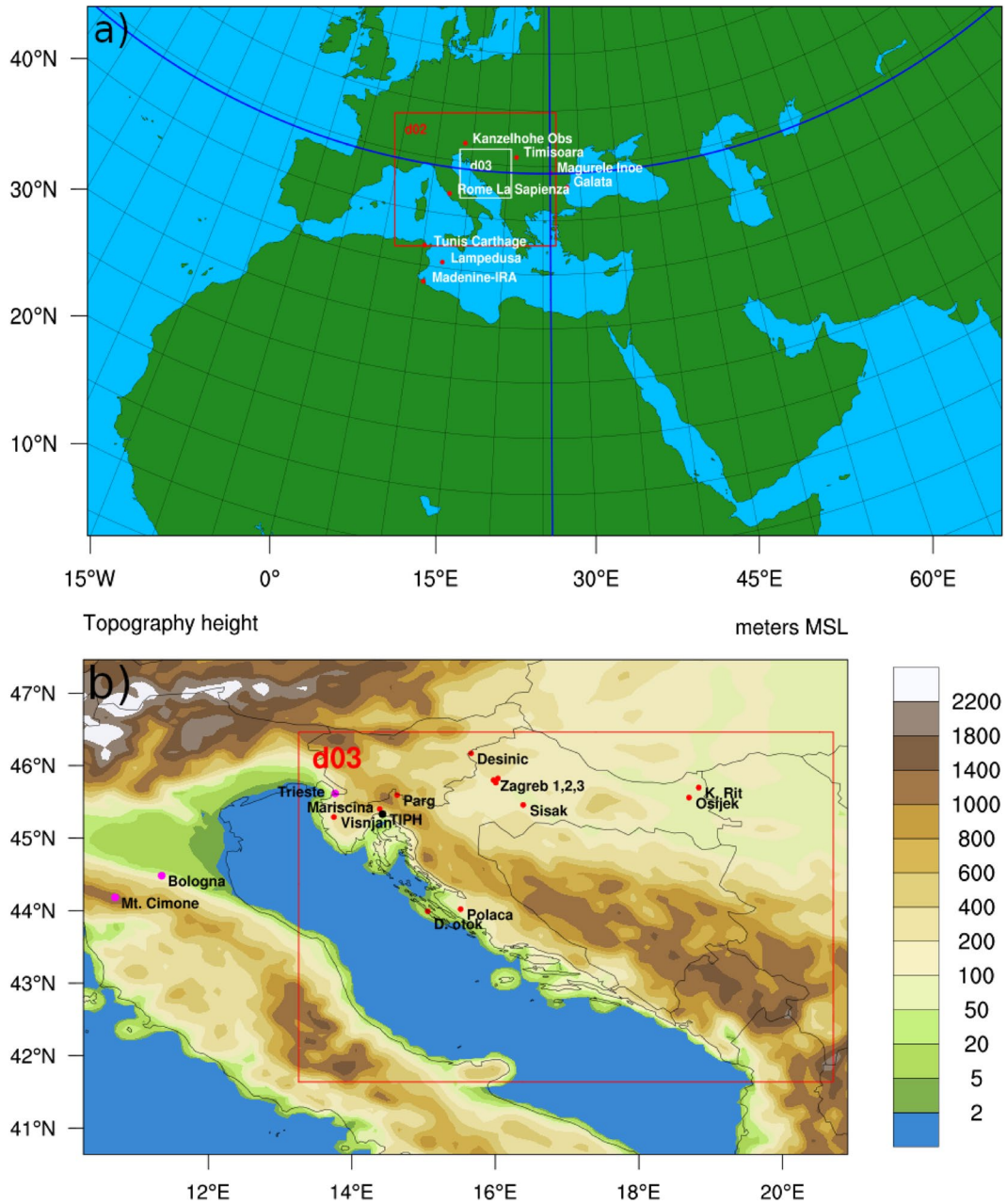

Figure 1. (a) The three nested WRF-Chem domains (d01, d02, d03) including the locations of the AERONET stations and the lines where the vertical cross sections are made (Figure 5); (b) the topography map of the finest model domain (d03) including the locations of the Croatian air quality stations (red dots) with available hourly PM_{10} measurements and the TIPH station (black dot) where the chemical analyses of the dust samples were performed. The blue lines in (a) represent the bases of the vertical cross sections in Figure 5.

with HYSPLIT trajectories and reanalyses of synoptic (e.g., ERA5) and particulate matter (PM) products, found the origin of dust particles near Lake Aral. However, their results from the trajectories and analysis of PM_{10} concentrations (their Figure 2 and Figure A3) suggest that the transport from the east was preceded by a transport from the Sahara that began on 25 March, while the merging of the two dust plumes over the Adriatic occurred in the evening hours of 26 March 2020. This could affect the more southern latitudes (i.e., the area of southern Italy and the broader area of the Balkan Peninsula), but this was not the subject of the study. This raises the question of the complexity of this event and the possible combined effects of transport from multiple regions into the central Mediterranean, which has not yet been uncovered. Preliminary results

Table 1
The List of Chosen Parameterizations in WRF-Chem Model

Parameterization	Choice of the scheme in WRF-Chem
Short wave radiation	Radiative Rapid Transfer Model (Iacono et al., 2008)
Long wave radiation	Radiative Rapid Transfer Model (Iacono et al., 2008)
Land surface model	Noah Land Surface Model (Chen & Dudhia, 2001)
PBL parameterization	MYNN Level 2.5 (Nakanishi & Niino, 2009)
Surface layer	MYNN (Nakanishi & Niino, 2009)
Microphysics	Morrison Double Moment (Morrison et al., 2005)
Dust emission	GOCART (Ginoux et al., 2001)

by Mifka et al. (2022a) for the Rijeka metropolitan area on the Adriatic coast suggest that there was a Saharan contribution to this extreme event.

Therefore, considering the unclear dynamics of dust transport in the Adriatic region, the purpose of this study is to further investigate this extremely rare event. The main objective is to answer the question whether there are contributions from different sources (Aral and/or Saharan region), as well as the meteorological background for their formation. Another objective is to find out if a coupled numerical model system is able to simulate this type of event. The detailed analysis was carried out using a different methodology than in previous studies (e.g., Strelec Mahović et al., 2020; Tositti et al., 2022), which can reveal the potential additional impact of the Saharan source. Accordingly, the present study consists of two main parts: (a) the coupled numerical simulations of atmospheric air quality, and (b) the chemical analysis and scanning electron microscope images (SEM) of PM_{10} filters. Those filters were collected during the March 2020 dust event at the air quality station in the city of Rijeka, Croatia, on the northeastern Adriatic coast (the TIPH station in Figure 1b). The coupled modeling framework is widely applied to dust transport issues (Grell et al., 2005; Palacios-Peña et al., 2019; Rizza et al., 2017; Skamarock et al., 2008, 2019; Teixeira et al., 2016), but to our knowledge, this is the first numerical simulation-based analysis of dust transport over the larger area of the eastern Adriatic Sea with fine resolution.

2. Materials and Methods

2.1. WRF-Chem Setup

The Weather Research and Forecasting (WRF) model version 3.7.1 (Skamarock et al., 2008, 2019) coupled with the Chemistry model (WRF-Chem; Grell et al., 2005) was used to simulate the dust episode. The coupled WRF-Chem model system is often used for general PM_{10} concentration evaluations (e.g., Gašparac et al., 2020) and/or specifically for dust transport events, but studies for Europe and the Mediterranean region generally focus on dust advection from the Sahara (e.g., Palacios-Peña et al., 2019; Rizza et al., 2017; Teixeira et al., 2016). The WRF model (Skamarock et al., 2008, 2019) was used to study the impact of the drying of the Aral Sea on climate and the effect of substantial air heating over the surface of the dried lake during summer in Roy et al. (2014) and Sharma et al. (2018), where a decrease in rainfall during winter was observed. Several dust WRF-Chem simulations have been performed for the Aral Sea (e.g., Karami et al., 2021; Li & Sokolik, 2018), suggesting that the model system is well-tested for simulations of this type and argues for reliable use in this study.

Therefore, three nested domains are used here in online mode with a resolution of 27×27 km^2 (d01), 9×9 km^2 (d02), and 3×3 km^2 (d03) at 51 vertical levels. The outer domain (d01) has 370×200 points over a larger area that includes North Africa, Central Asia, and Europe (Figure 1). The simulation begins on 19 March 2020 at 12 UTC and ends on 31 March 2020 at 18 UTC. The first 3 days were taken for the spin-up and discarded during the evaluation. The meteorological boundary conditions are from the European Centre for Medium-Range Weather Forecasts (ECMWF) operational analysis with a resolution of $0.125° \times 0.125°$ (ECMWF, 2020).

The physical processes in the model are simulated by selecting the available parameterizations (Table 1). The Mellor-Yamada-Nakaniski and Niino (MYNN) scheme at level 2.5 with prognostic TKE was chosen for the parameterization of turbulence in the PBL and surface layer (Nakanishi & Niino, 2009). The Radiative Rapid Transfer Model (Iacono et al., 2008) for long and short wavelength radiation was used as the radiation scheme.

10.1029/2023EA002879

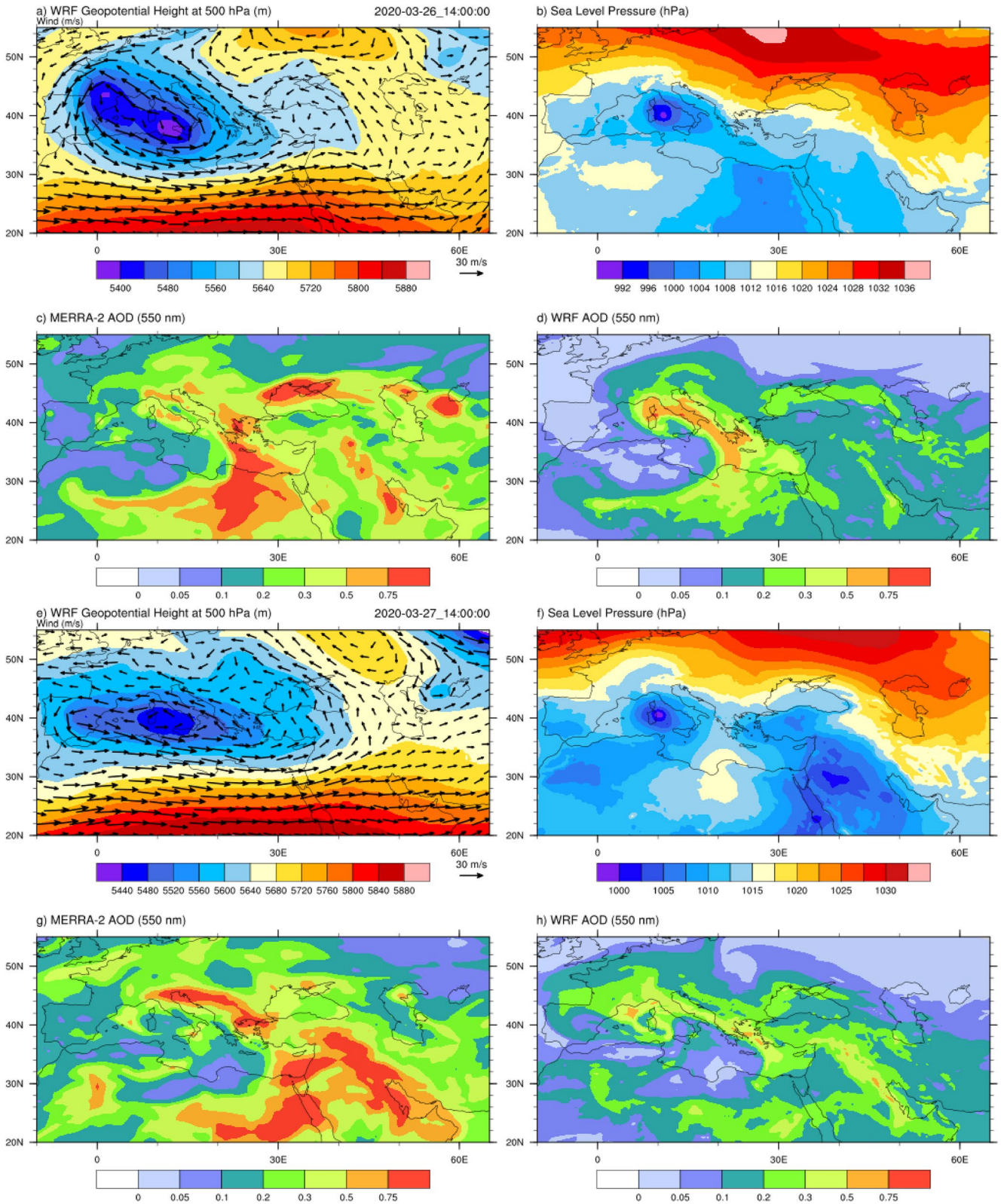

Figure 2. Geopotential and wind at 500 hPa (a, e), sea level pressure (b, f), AOD at 550 nm from MERRA-2 reanalysis (c, g), and WRF-Chem (d, h) during the dust outburst on 26–27 March 2020 at 14 UTC.

The Morrison Double Moment Scheme (Morrison et al., 2005) was used for the microphysical processes in the model. The Noah Land Surface Model (Chen & Dudhia, 2001) was chosen for the land surface model: A Unified NCEP/NCAR/AFWA Scheme with soil temperature and moisture in four layers. Nudging of wind, temperature, and moisture toward the boundary conditions in the model is applied to reduce the errors (Kumar et al., 2014; Lo et al., 2008) by using four-dimensional data assimilation (FDDA). The nudging (FDDA) is omitted in PBL to avoid the interference with mesoscale forcings in the model, which is important for PBL development (Choobari et al., 2012; Cremades et al., 2016).

To represent aerosols in this simulation, the Georgia Tech/Goddard Global Ozone Chemistry Aerosol Radiation and Transport (GOCART) model (Ginoux et al., 2001) was chosen (chem_opt = 300). This module simulates five major tropospheric aerosols: sulfate, organic carbon, black carbon, dust, and sea salt. Dust is represented in five fractionated bins with an effective radius ranging from 0.73 to 8.0 μm. There are three different options for the dust emission models implemented in this module. Although the dust emission scheme GOCART-AFWA (dust_opt = 2) is the improved scheme that incorporates the more physically realistic saltation flux parameterization (LeGrand et al., 2019), the scheme GOCART-WRF is used in this study (dust_opt = 1). The main reason for this choice is related to the evaluation of the model's performance, which is explained in Section 3.2. The dust emission in the GOCART-WRF scheme is based on the formulation of Gillette and Passi (1988), which is based on the surface wind speed and the threshold velocity of wind erosion:

$$F_p = \begin{cases} C S s_p u_{10\mathrm{m}}^2 (u_{10\mathrm{m}} - u_t) & \text{if } u_{10\mathrm{m}} > u_t \\ 0, & \text{otherwise} \end{cases} \quad (1)$$

where F_p (kg m^{-2} s^{-1}) is the emission flux of each size class p, C (kg m^{-5} s^2) is the empirical constant that is not changed here (e.g., Kumar et al., 2014), s_p is the fraction of each size class in the emission, $u_{10\mathrm{m}}$ (m s^{-1}) is the horizontal wind speed 10 m above the surface. Emission occurs only when $u_{10\mathrm{m}}$ is above the threshold velocity u_t, which is a function of particle size, air density, and surface moisture. The details of the threshold velocity (u_t) calculation can be found in Ginoux et al. (2001). S here stands for the source function, a simplification used in the GOCART model due to the lack of alluvial data. The source function is based on the assumption that basins with pronounced topographic variations contain sediments that have accumulated in valleys and depressions. S is the probability that the accumulated sediments are in grid cell i of elevation z_i, and $z_{\max}$ and $z_{\min}$ are the maximum and minimum elevations, respectively, at 1° × 1° resolution in the surrounding 10° × 10° topography. The size of this range was chosen because most hydrologic basins in arid regions have a size of 10° × 10°. Therefore, the resulting expression for S is:

$$S = \left(\frac{z_{\max} - z_i}{z_{\max} - z_{\min}} \right)^5. \quad (2)$$

In WRF-Chem, the global distribution of S is part of a static geographic field of the WRF Preprocessing System (WPS). There are two additional parameterizations for dust emission in WRF-Chem, but for this episode, the preliminary results significantly overestimated the observed PM_{10} levels and were therefore discarded in this study. The removal of dust from the atmosphere is composed of dry and wet deposition. Dry deposition considers turbulent transfer and deposition by gravity, while wet deposition includes rainout and washout in and under clouds. For more details, see Chin et al. (2000) and Ginoux et al. (2001).

2.2. Sources of the Aerosol Optical Depth Data (MERRA-2 Reanalysis and AERONET AOD)

The optical properties were used here to identify the dust plumes and to check the performance of the WRF-Chem simulations. In particular, the Aerosol Optical Depth (AOD) observed by the Moderate Resolution Imaging Spectroradiometer (MODIS) aboard the Aqua satellite (MYD04_L2) operated by NASA is used here to qualitatively describe this dust event (Levy et al., 2015). The final product is the layer created as a combination of the Dark Target (Kaufman et al., 1997) and Deep Blue (Hsu et al., 2004) algorithms for the land and ocean. The sensor/algorithm resolution is 10 km in nadir, the image resolution is 2 km in nadir, and the temporal resolution is daily. Satellite data can be used to identify the evolution and position of dust plumes, but uncertainties in the measurements arise from clouds or the high content of water vapor in the column (Schepanski et al., 2012), in

this case especially over the area of interest during the dust episode. Therefore, the AOD product of Modern-Era Retrospective Analysis for Research and Applications, version 2 (MERRA-2; Buchard et al., 2017) was also used (GMAO, 2015a). MERRA-2 is based on the Earth system model NASA Goddard Earth Observing System, version 5 (GEOS-5) (Molod et al., 2015), which is coupled with the Goddard Chemistry Aerosol Radiation and Transport model (GOCART; Colarco et al., 2010) that simulates five types of aerosols, including dust, sea salt, sulfate, black, and organic carbon. Using the three-dimensional variable data assimilation (3Dvar) Grid-point Statistical Interpolation Analysis System (GSI) (Kleist et al., 2009), the AOD is assimilated from both the satellite and ground-based measurements. The aerosol optical depth (AOD) is assimilated by MODIS (from the Terra and Aqua satellites) and the Advanced Very High-Resolution Radiometer (AVHRR) after bias correction. The uncorrected AOD is taken by the space-based Multiangle Imaging SpectroRadiometer (MISR) over bright surfaces and by ground-based Aerosol Robotic Network (AERONET) stations. Aerosol data from the MERRA-2 reanalysis have been verified in several studies (e.g., Buchard et al., 2017; Kok et al., 2021a; Reichle et al., 2017; Wu et al., 2020) at a number of stations around the world for several decades. In addition, MERRA-2 fields for sea level pressure and 500 hPa geopotential (GMAO, 2015b) were used to analyze synoptic conditions.

To compare the WRF-Chem AOD with observations, data from eight AErosol RObotic NETwork (AERONET) stations located downwind of dust plumes from the East and Sahara (i.e., four stations in the Balkans and 4 stations in the Mediterranean) were used. AERONET is a worldwide network of solar photometer stations that measure the spectral extinction of direct radiation according to the Beer-Lambert-Bouguer law (Holben et al., 1998). This study uses version 3 AOD data calculated at quality level 2.0 (quality assured) for both stations. AOD from WRF-Chem is available at four wavelengths (300, 400, 600, 999), while measurements are available at several different wavelengths (Holben et al., 1998). To compare the modeling results, the Ångstrom power law (as in the work of Kumar et al., 2014) is applied to the WRF chem AOD at 500 nm (for Lampedusa) and 510 nm (for Galata station).

2.3. PM_{10} Observations and Chemical Analysis

Daily PM_{10} concentration and chemical analysis were obtained from the quartz filter sampled for 24 hr on 27 March 2020, at the Teaching Institute of Public Health in Rijeka (TIPH, 45°19′54″N, 14°25′32″E, 32 m a.s.l., Figure 1b). The concentration was determined by the gravimetric method after the filter was prepared and weighed in the weighing room under controlled conditions of relative humidity (45%–50% RH) and temperature (19–21°C). The filter was cut into eight pieces, which were used for the different analyses. Heavy metal concentrations (Pb, Cd, Cu, Zn, Fe, Mn) were obtained from the process of mineralization of the filter and then analyzed using ICP-MS (Inductively Coupled Plasma Mass Spectrometry, NexION 300X, Perkin Elmer). A detailed explanation of this procedure can be found in Mifka et al. (2021). The other parts of the filter were used for the analysis of polycyclic aromatic hydrocarbons (PAHs) and SEM. Individual PAHs were determined by filter extraction in spectrograde cyclohexane, purification of the extract on the silica gel column, and quantitative determination by HPLC with coupled UV/fluorescence detector (further details in Alebić-Juretić, 2015). The PAHs analyzed for this study are: naphthalene (Nap), acenaphthene (Ace), fluorene (Fln), phenanthrene (Phe), anthracene (Anth), fluoranthene (Flo), pyrene (Py), chrysene (Chr), benzo(a)anthracene (BaA), benzo(b)fluoranthene (BbF), benzo(k)fluoranthene (BkF), benzo(a) pyrene (BaP), indeno(1,2,3-c,d)pyrene (IP), dibenzo(a,h)anthracene (DBA), and benzo(g,h,i)perylene (BghiPe). Hourly PM_{10} levels from the 12 air quality stations (locations in Figure 1b) of the Ministry of Economy and Sustainable Development (http://iszz.azo.hr/iskzl/index.html) were used for model verification.

2.4. HYSPLIT Trajectories

To determine the area of dust sources, HYSPLIT (HYbrid Single-Particle Lagrangian Integrated Trajectory) back trajectories (Stein et al., 2015) were calculated using the web-based Real-time Environmental Applications and Display sYstem (READY) (Stein et al., 2015). The meteorological fields used to calculate the trajectories were taken from the archived NCEP Global Assimilation System (GDAS) model with a resolution of 1° × 1°. For this purpose, HYSPLIT 72-hr backward trajectories were computed on 27 March at 12 and 18 UTC, terminating over Zagreb (Croatia) at 1,400 m a.g.l. and 5,000 m a.g.l., respectively.

2.5. SEM

Morphological characterization was performed using an SEM JSM-7800F (Jeol Ltd., Japan) equipped with an energy dispersive X-ray spectrometer (EDS) for qualitative X-ray analysis. For SEM observations, a portion of

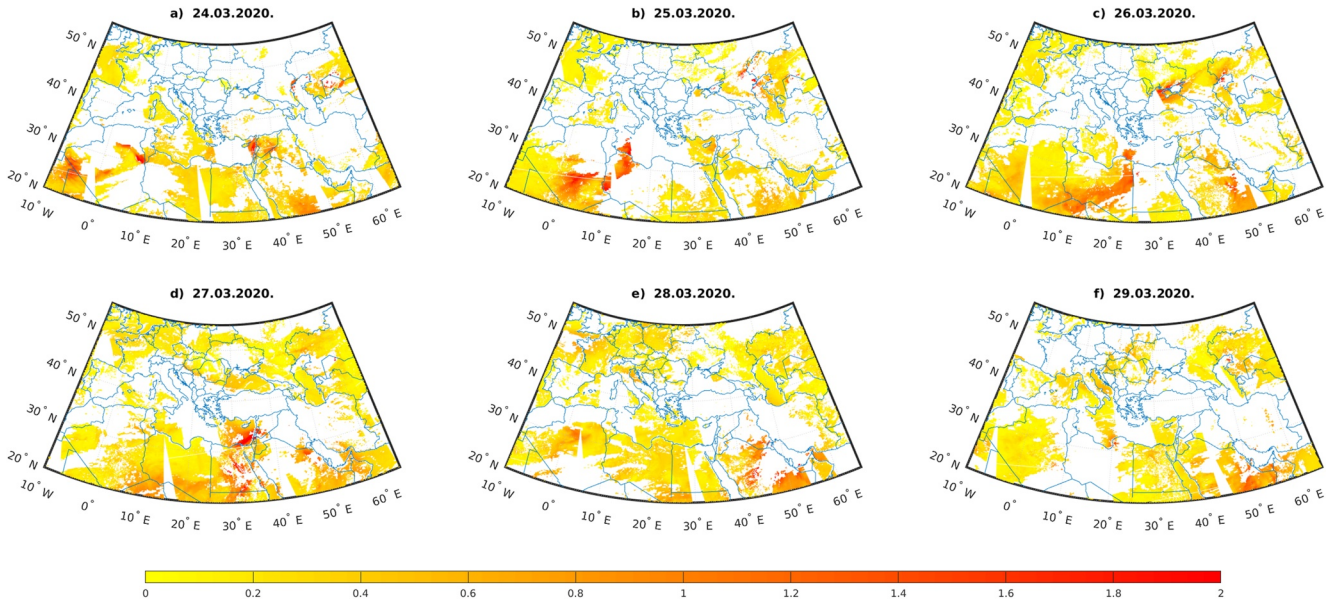

Figure 3. The daily maps of MODIS/AOD at 550 nm during the dust event from: 24 March 2020 (a) to 29 March 2020 (f).

the filter was gently pressed onto a conductive carbon adhesive tab attached to the sample holder to transfer the filter contents. The sample was then coated with a gold/palladium layer approximately 10 nm thick using the Precision Etching and Coating System, PECS II (Gatan Inc., CA, USA). The surface morphology of the particles was studied by collecting the secondary electrons with an accelerating voltage of 5 kV. The elemental composition of some particles was determined from EDS analysis using an Oxford Instruments X-Max 80 mm2 detector with the SEM accelerating voltage of 25 kV.

3. Results and Discussion

3.1. The Case Description

The exceptional increase in particulate matter concentrations was recorded at the TIPH station on 27 March. In particular, the PM_{10} concentration measured by a gravimetric method at the TIPH station was 216.3 μg m^{-3}, which is significantly higher than the average concentration for 2020, which was 28 μg m^{-3} and calculated for a total of 72 measurements. It is also the highest measured value for that year, while the 98th percentile was 59 μg m^{-3}. It is also worth noting that only two measurements in 2020 at this station were above the limit. This information is taken from the TIPH report at https://zzjzpgz.hr/publikacije/kvaliteta-zraka-na-podrucju-pgz-u-2020/ (written in Croatian). The synoptic situation preceding the dust transport shows the development of systems responsible for transport from both North Africa and the East. On 23–24 March 2020, the upper-level trough is present over Europe with an axis aligned in NE-SW direction from Russia to Sardinia. At the surface, most of Europe is under the influence of the anticyclone with the center over the Baltic Sea. At the same time, the trough over NW Africa and Spain is connected with a surface cyclone having 1,005 hPa at its center (Figure SA1 in Supporting Information S1).

This cyclone is known as a Sharav cyclone (Alpert & Ziv, 1989), which typically occurs in the spring due to the increased baroclinic temperature gradient between North Africa and the Mediterranean Sea. As in this case, it moves rapidly along the North African coast, lifting the Saharan dust. On 25 March 2020, in the south of Europe, the upper-level cut-off-low in retrograde movement extended in the SW direction. Therefore, the cyclonic flow continues and enables the surface Sharav cyclone to relocate to the central Mediterranean where it deepens. This situation favors the transport of Saharan dust. The strong pressure gradient between the Mediterranean cyclone and the anticyclone to the north is the main factor in dust transport from the east. Both dust plumes were present on 26 and 27 March 2020 (Figures 2 and 3), which can be seen when observing the AOD fields. During the afternoon hours of 26 March (Figure 2c), the two plumes are clearly visible. At this time, it can be seen that the AOD of WRF-Chem is overestimated over Italy and underestimated over the Balkans.

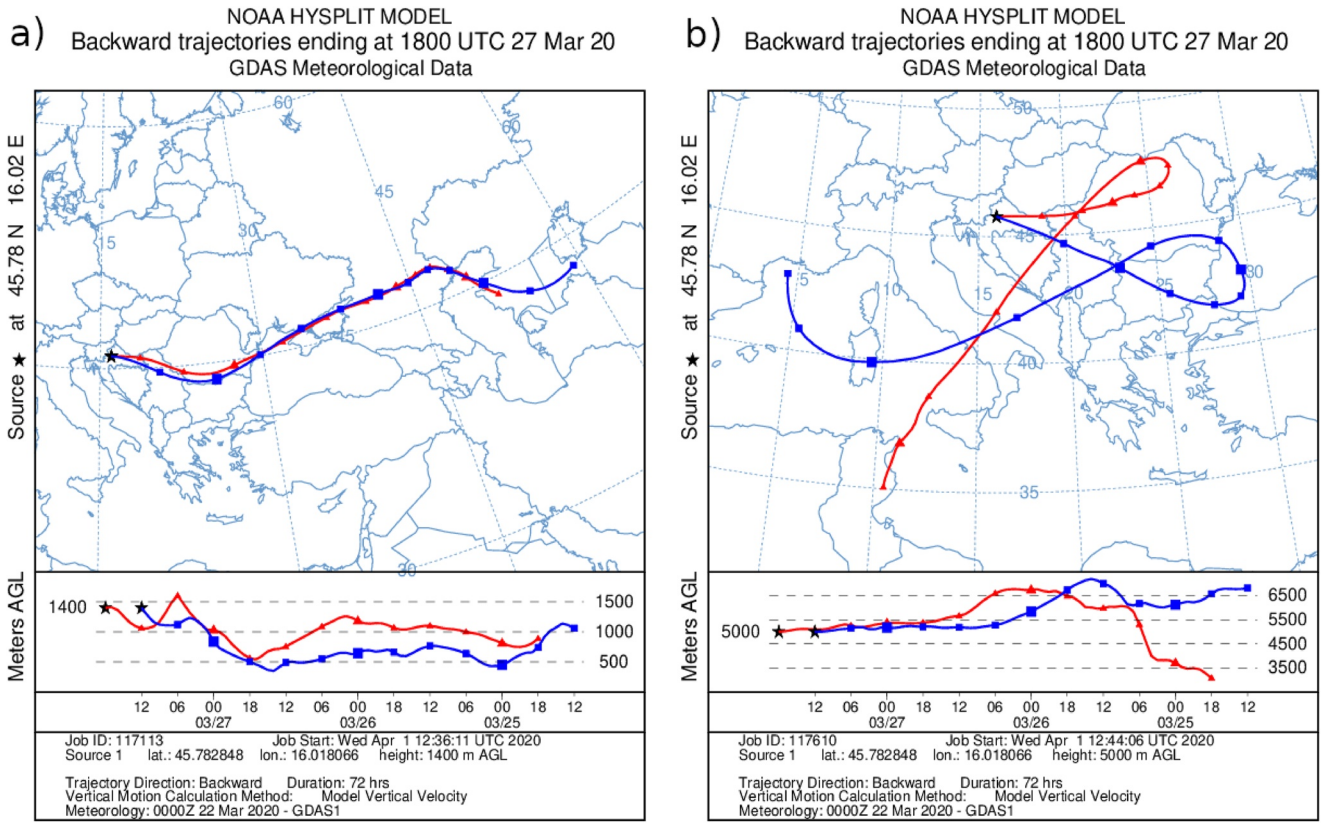

Figure 4. HYSPLIT 72-hr backward trajectories on 27 March at 12 (blue lines) and 18 (red lines) UTC observed over Zagreb (Croatia) at: (a) 1,400 m a.g.l. and (b) 5,000 m a.g.l.

The primary source of AOD fields here is the MODIS/AOD at 550 nm (Figure 3). On 24–25 March, the elevated AOD levels observed east of the Caspian Sea indicate strong emissions in the area encompassing the Aral Sea. This event is confirmed and briefly described at: https://earthobservatory.nasa.gov/images/146487/a-dusty-day-over-the-aral-sea. The development of a dust plume and the aforementioned horizontal merger with the Saharan dust can be seen in Figures 3c and 3d. However, much of the Balkan region was obscured by clouds during these days. Therefore, the MERRA-2 reanalysis AOD proved to be the perfect tool to fill in the missing gaps and also to evaluate the goodness of the AOD simulated by WRF-Chem (Figure 2).

Although the HYSPLIT and WRF models can indicate a similar result, Lagrangian and Euler approaches are fundamentally different and can complement each other well, especially when they converge to a similar result. In our case, HYSPLIT (Lagrangian approach) offers the possibility to extract dust contributions from two geographically quite distant sources, which would not be easily observed with purely Eulerian models (MERRA-2 and WRF-Chem). The backward trajectories of HYSPLIT confirm the existence of two dust plumes merging over a larger area in the Balkans (Figure 4). According to the measured PM_{10} values in Zagreb, the concentration peak was in the early afternoon hours of 27 March, and therefore two trajectories with end times at 12 and 18 UTC were chosen at this location. The trajectories up to ~4,000 m a.g.l. can be attributed to transport from the east, and the layer with the fastest advection was found between ~1,350 and 1,750 m a.g.l. (Figure 4a). The corresponding trajectories terminate within the mixed layer as the temperature inversion begins at 1,600 m at 12 UTC (Figures SA2 and SA3 in Supporting Information S1). Moreover, these trajectories cross the desert area between the Caspian Sea and the Aral Sea on 24–25 March, when dust emission occurred due to the elevated AOD in this area. The height of trajectories in this area is also within the PBL (Figures SA2 and SA3 in Supporting Information S1). Trajectories that terminate above ~5,000 m a.g.l. (Figure 4b) indicate the advection of dust from North Africa in the upper level, coinciding with the shift of the Sharav cyclone in the Tyrrhenian Sea (Figure 2). Moreover, the aforementioned trajectories form a loop over the broader Balkans (Figure 4b) during the (approximate) period from 25 March 2020 at 12 UTC to 27 March 2020 at 18 UTC, while the Asian dust plume occurs in the same

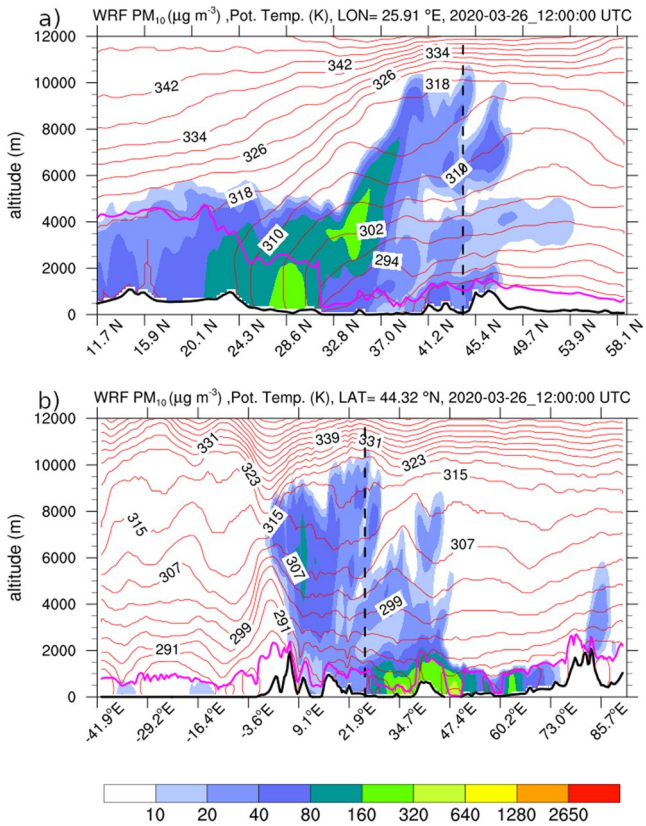

Figure 5. Modeled vertical crosssections of PM_{10} dust concentration (colored areas), potential temperature (red lines), PBL height (cyan line), and topography (black line) for 26 March 2020 at 12 UTC: (a) meridional, and (b) zonal at the approximate location of Bucharest, Romania, marked with blue lines in Figure 1a.

area on 26 March 2020 at 18 UTC. Looking at the situation horizontally and focusing on the highest measured PM_{10} levels, the Saharan dust was present ~1 day before the Asian one, and both plumes were present over the same part of the Balkan Peninsula on 26 March 2020. Our results are consistent with the study by Tositti et al. (2022), which found that the two dust plumes merged on the evening of 26 March (their Figures 1c, 2c, A1c).

The conclusion from this analysis, then, is that two dust plumes mixed over the Balkans east of Zagreb, but the question of the extent of the relative influence of the two sources remains open. The (partial) answer to this question can be provided by the chemical and SEM analysis, which will be presented later in Sections 3.3 and 3.4. According to the analysis of the back trajectories, with end times during the peak concentrations, the presence of Saharan dust over the Balkans is longer, but the advection occurs at higher levels and over the PBL (Figure 5a). The vertical structure of meridional and zonal advection at the Bucharest site (Figure 1) provides further information. According to the HYSPLIT results, the Asian dust plume can be assumed to be advected below 2000 m. Therefore, from the vertical cross sections, it can be inferred that the first occurrence of the Asian plume actually took place on 25 March 2020 at 18 UTC (Figure 5), but the advection occurred above the PBL. Due to the PBL height increase, the "first Asian dust" within the PBL was in the morning hours on 26 March 2020 and coincided with the trajectory that ended in Zagreb at 12 UTC (Figure 6). Therefore, the highest PM_{10} peak over Zagreb was associated with the Asian dust source.

3.2. Evaluation of WRF-Chem PM_{10} and AOD With Ground-Based Measurements

In addition to the PM_{10} increase observed at the TIPH station, hourly values at several air quality stations in Croatia (Figure 7) and surrounding countries (not shown) provide further evidence of this unusual dust outbreak. Therefore, the performance of the WRF-Chem model for PM_{10} concentrations at the lowest model level in the finest range (d03) is validated with measurements provided by in situ air quality stations in Croatia using the nearest neighbor method. To assess the model's capabilities, a number of statistical parameters were calculated and compared (similar to Gašparac et al. (2020))

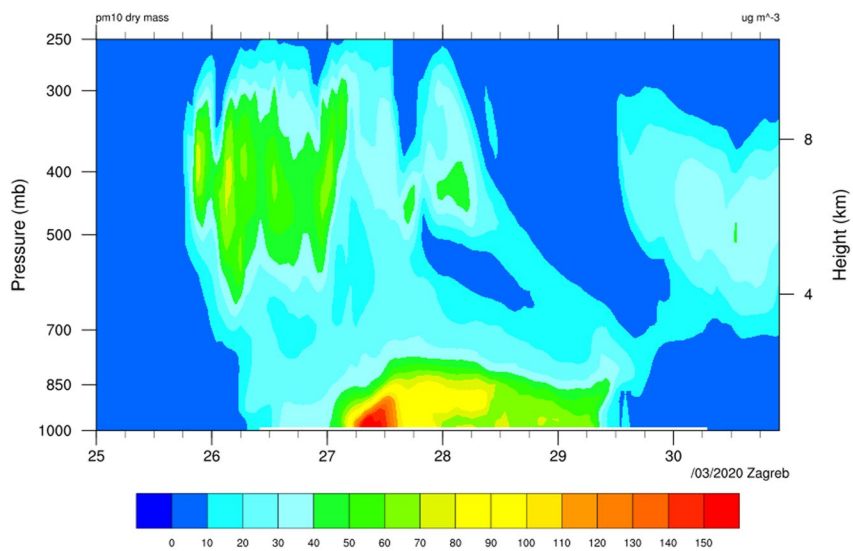

Figure 6. Time-height plot of the PM_{10} concentrations at a location near Zagreb.

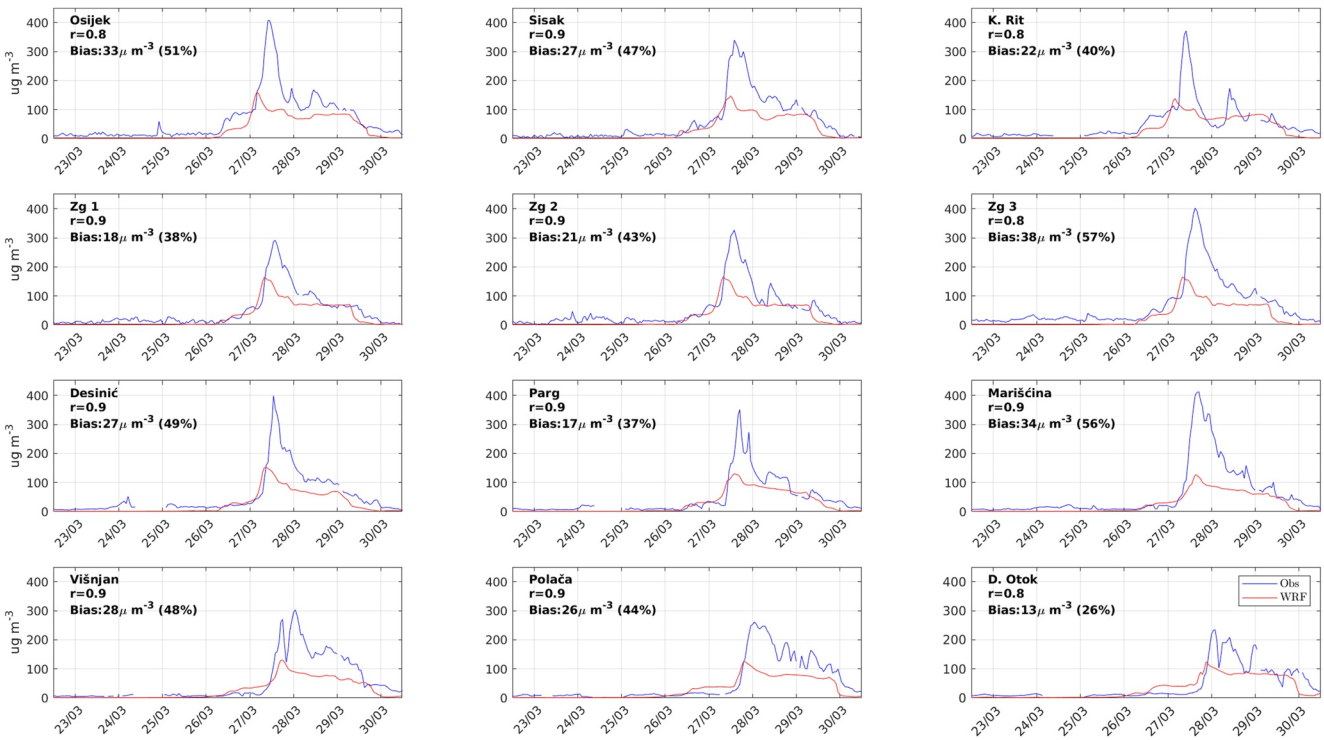

Figure 7. Time series of observed and modeled PM_{10} concentrations (μg/m^3) at Croatian stations (locations are shown in Figure 1b) from 22 March 2020 to 1 April 2020 (at 12 UTC).

for the period 22–30 March starting and ending at 12 UTC: the standard deviations of modeled (σ_m) and observed (σ_o) PM_{10} concentrations, the root mean square error (RMSE), the root mean square error after removal of a constant bias (RMSD), and the bias and correlation coefficients (R). The following criteria (e.g., Kehler-Poljak et al., 2017; Pielke & Mahrer, 1978; Teixeira et al., 2014) were applied to measure the success of the model: (a) $\sigma_m \approx \sigma_o$, (b) RMSE $\lesssim \sigma_o$, and (c) RMSD $\lesssim \sigma_o$. According to the obtained ratios and the given criteria, the overall performance of the model to capture the dust event is satisfactory (Table 2, Figure 7). Except for the underestimation of PM_{10} concentrations and AOD, the modeled results agree acceptably. The modeled σ_m is less than twice the measured σ_o at most stations. It is important to emphasize that although anthropogenic emissions and

Table 2
Verification of WRF-Chem PM_{10} With the Measurements at Stations (μg/m^3)

Stat.	<PM_o>	<PM_m>	σ_o	σ_m	RMSE	RMSD	σ_m/σ_o	RMSE/σ_o	RMSD/σ_o	R	BIAS
Osijek	65.3	32.2	78.9	40.7	60.5	50.7	0.5	0.8	0.6	0.8	33.1
Sisak	57.7	30.5	75.6	39.7	51.5	43.8	0.5	0.7	0.6	0.9	27.1
K. Rit	53.8	32.2	64.2	37.7	48.4	43.3	0.6	0.8	0.7	0.8	21.6
Zg 1	46.4	28.6	60.9	40.2	36.6	32	0.7	0.6	0.5	0.9	17.8
Zg 2	49.8	28.5	66.1	40	43.8	38.2	0.6	0.7	0.6	0.9	21.3
Zg 3	67.2	28.9	82.6	40.4	65.9	53.6	0.5	0.8	0.6	0.8	38.3
Desinić	55.3	28.3	72.6	38.3	51.7	44.1	0.5	0.7	0.6	0.9	26.9
Parg	47.4	30	64.2	37.1	40.4	36.5	0.6	0.6	0.6	0.9	17.4
Marišćina	60.2	26.6	92.2	33.7	71.6	63.2	0.4	0.8	0.7	0.9	33.7
Višnjan	58.2	30.5	76	34.6	54.3	46.7	0.5	0.7	0.6	0.9	27.7
Polača	59.1	33.3	74.3	36	53.2	46.6	0.5	0.7	0.6	0.9	25.8
D. Otok	48.7	36.1	59.2	36.3	39	36.9	0.6	0.7	0.6	0.8	12.5

complex chemistry are not included in this model simulation, the RMSD and especially the RMSE are not much different from σ_o (Table 2).

Not taking anthropogenic emissions into account can probably explain the existing bias, but only partially. Furthermore, if we compare the AOD during the dust emission period (Figure SA1 in Supporting Information S1), we can conclude that WRF-Chem underestimates the dust emission. Several studies show that the MERRA-2 AOD fields have the best performance among the different models compared to the observations (Kok et al., 2021a; Wu et al., 2020.). However, in general, surface concentrations and deposition are often overestimated in the models because they use the spherical approximation of aspherical dust particles (Kok et al., 2021a). On the other hand, the emission and lifetime of coarse dust particles (5 < diameter <20 μm) are usually underestimated. In this study, the GOCART model has the largest particle with an effective diameter of 16 μm. An additional problem with most models is the occurrence of bias in dust loading over dust sources (Kok et al., 2021a; Ridley et al., 2016). This study confirms this fact. Qualitatively, it can be inferred that during the emission process, the AOD over dust sources is lower in the WRF-Chem results than in those from MERRA-2 (Figure SA1 in Supporting Information S1). The desert dust sources areas are approximated by the HYSPLIT trajectories, but the underestimation can be seen over a larger/total simulation area. As mentioned in Section 2.1, the representation of dust sources in the GOCART model is based on a simple source function (Equation 2) that covers a large area (10° × 10°) and is computed from elevation data with a resolution of 1° × 1°, which is appropriate for large-scale regions such as the Sahara. In the study by Cremades et al. (2016), it was shown that the default erodibility map in WRF-Chem leads to an underestimation of dust emissions in smaller regions when the simulations are performed at fine resolution. This fact is the most likely explanation for the underestimation of AOD and PM_{10} in this simulation, especially because the erodibility over the Aralkum desert is zero. Gašparac et al. (2020), in evaluating PM_{10} concentrations in WRF-Chem air quality simulations, also noted that the underestimated modeled PM concentrations in some cases indicated the importance of accurately assessing regional air pollution transport under statically stable atmospheric conditions common to anticyclonic conditions. In addition, the sensitivity test was conducted using the GOCART-AFWA dust emission scheme while retaining the other parameterizations. This test resulted in a significant overestimation of PM_{10} measurements, while the correlation was comparable to the case where the GOCART-WRF scheme was applied. Since the sensitivity tests were out of the scope of this work and the GOCART-WRF scheme showed better results, it was used for further analysis.

To evaluate the model over a larger area, the WRF-Chem AOD was compared to the AERONET network AOD time series observed at eight stations. The stations were selected based on their location relative to the Asian and African dust transport pathways (Figure 8). This comparison with in situ observations further confirmed that the model underestimates AOD. It is most severely underestimated at stations on the Balkan Peninsula, where, for example, the observed values at Galata station on 27 March 2020 were up to ∼3.14 times higher than those of the model (the observed AOD at 4:50 UTC was 0.72, while the WRF-Chem AOD was 0.23). Although observations are mostly absent (due to cloud cover) during 25–26 March 2020, when transport from the Sahara occurred, the simulations appear to better match observations at stations in the Mediterranean region. Since most of these stations are in the relative vicinity of dust sources, the increase in AOD can be roughly attributed to mineral dust during the outbreak. In addition, other factors such as soil moisture simulation may also be the cause of the bias (e.g., Sardoo et al., 2022).

3.3. Chemical Signature of PM_{10}

Chemical analyses of dust samples were performed to better identify possible sources, that is, to evaluate the presence of typical Saharan dust markers and the possible presence of pollutants associated with the different air masses. During the intense dust intrusion in the northeastern part of the Adriatic Sea, PM_{10} concentrations up to 7 times higher than usual (216 μg/m^3) were measured at the TIPH station (location visible in Figure 1b) (Table 3). The concentration of metals (Pb, Cd, Cu, Zn, Fe, Mn) shows increased values of Fe (2.676 μg/m^3) and Mn (3.495 μg/m^3) compared to samples collected before and after the intense dust event (Table 3). These concentrations are also several times higher than those normally measured in the same area (Mifka et al., 2021). Normally, the concentrations of Fe and Mn, as well as Ca and Ti, are higher during Saharan dust advection than the annual mean values for a given area (Federici et al., 2018). The total concentration of PAH of 2.636 μg/m^3 was within the range of values previously measured at the same site without dust intrusion (Table 4). Significantly higher

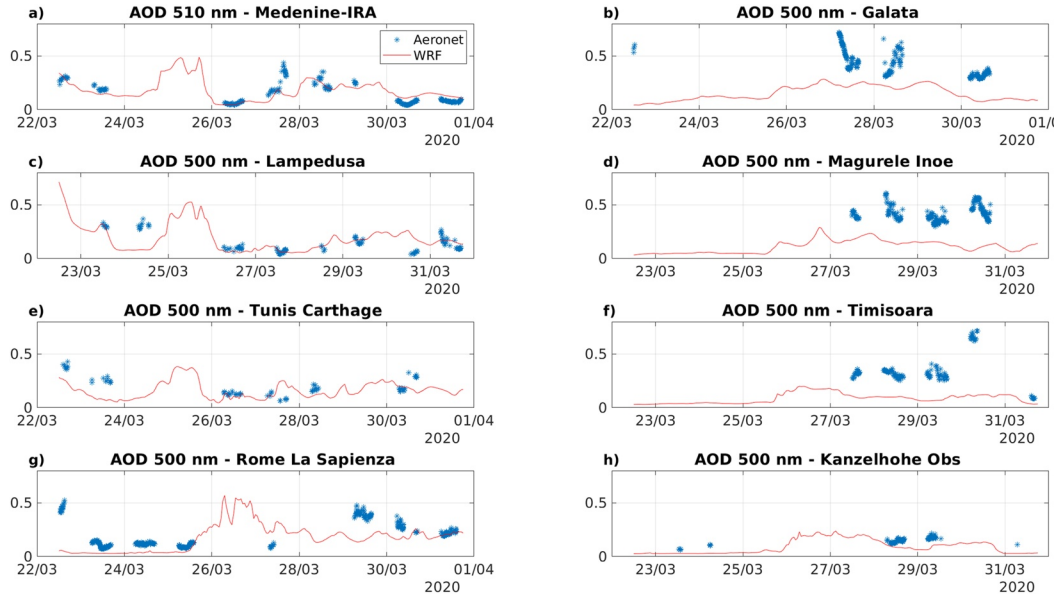

Figure 8. Time series of observed and modeled AOD values at eight stations along the Sahara plume path (a, c, e, g) and along the eastern plume path (b, d, f, h) (locations are shown in Figure 1) from 22 March 2020, at 12 UTC to 31 March 2020, at 18 UTC.

values were measured for BbF, BkF, Chr, and IP. BbjF and Bghip are the predominant PAHs in ports and transects in the marine atmosphere of the southern and eastern Mediterranean Sea (Romagnoli et al., 2016). The diagnostic PAH ratios commonly used to identify sources (Bap/BghiP = 0.337 non-transport; Flo/Flo + Pyr = 0.31 gasoline emission; and Ant/Ant + Phe = 0.092 petrogenic source) suggest that the identified PAHs that survive chemical and photochemical degradation during long-distance transport are likely of petrogenic origin (Federici et al., 2018). Although the dust from the Aralkum desert area would also be expected to have elevated PAH levels because the area is considered polluted (O'Hara et al., 2000; Whish-Wilson, 2002), measured PAHs do not exhibit higher concentrations.

3.4. Mineral Phases of PM_{10}

SEM images (Figure 9; Figure SB1 in Supporting Information S1) of GFF filters containing PM_{10} confirm a morphology typical of glauberite ($Na_2Ca(SO_4)_2$) or $CaSO_4 \times 2H_2O$ desert rose gypsum (Figure 9a), aluminosilicate with embedded Fe (Figure 9c), calcite (Figure SB1a in Supporting Information S1), sodium chloride (Figure SB1b in Supporting Information S1), and primary biological aerosol particles (Figure 9d). Biological material (Figures 9b1 and 9b2) resembling the skeleton of a diatom was also visible in some images. The available mineralogical results are not necessarily sufficient to make an accurate source attribution, but the minerals identified suggest a predominantly Saharan origin, similar to what is suggested by the analysis of trace metals and PAHs. Dust from the Aralkum is mainly characterized by quartz, calcite, and dolomite (Groll et al., 2019).

Table 3
The PM_{10} and Metals Concentration ($\mu g/m^3$) of the Sample at the TIPH Station in Rijeka on 27 March 2020 (Shaded)

Date	PM_{10}	Pb	Cd	Cu	Zn	Fe	Mn
11/03	31.2	0.019	0.338	0.194	0.187	1.804	0.469
18/03	24.3	0.011	0.279	0.221	0.167	0.793	0.354
27/03	216.3	0.018	0.247	0.268	0.016	2.676	3.495
30/03	19.4	0.006	0.083	0.143	0.129	0.272	0.364

Note. In addition, analyses of the samples before and after intense dust event are given.

It is interesting that a very high concentration (up to 400 $\mu g/m^3$) of PM_{10} was measured in the Ljubljana area of Slovenia during the same intense dust event. Analysis of SEM (unpublished results, https://bojanambrozic.com/2020/04/02/analiza-puscavskega-peska-z-elektronskim-mikroskopom/) showed sand grain sizes ranging from less than 1 µm to more than 100 µm, with most being about 6 µm in size (so they are indeed PM_{10} particles). Chemical analysis of the individual grains showed that the sand was composed mainly of quartz grains, iron oxides and hydroxides, aluminum oxides, and various salts. The presence of fragments of individual microfossils, mainly diatoms, was detected among the sand grains, which is consistent with our results (in Figure 9b1/b2).

Table 4
The PM_{10} and Polycyclic Aromatic Hydrocarbons (PAHs) Concentration ($\mu g/m^3$) of the Samples at the TIPH Station in Rijeka on 27 March 2020 (Shaded)

Date	Unit	11/03	18/03	27/03	27/03	30/03
PM_{10}	($\mu g/m^3$)	31.2	24.3	216.3	216.3	19.4
Naph	(ng/m^3)	<0.003	<0.003	<0.003	<0.003	<0.003
Ace	(ng/m^3)	<0.002	<0.002	<0.002	<0.002	<0.002
Flr	(ng/m^3)	<0.007	<0.007	<0.007	<0.007	<0.007
PHE	(ng/m^3)	0.037	0.028	0.089	0.089	0.13
ANTH	(ng/m^3)	0.007	<0.003	<0.003	<0.003	0.004
FLO	(ng/m^3)	0.164	0.125	0.163	0.163	0.305
PY	(ng/m^3)	0.19	0.105	0.147	0.147	0.186
BaA	(ng/m^3)	0.033	0.052	0.092	0.092	0.076
Chr	(ng/m^3)	0.23	0.08	0.155	0.155	0.124
BbF	(ng/m^3)	2.205	0.416	0.805	0.805	0.47
BkF	(ng/m^3)	1.042	0.244	0.464	0.464	0.244
BaP	(ng/m^3)	0.545	0.142	0.173	0.173	0.098
DBA	(ng/m^3)	0.014	0.003	0.008	0.008	0.006
BghiP	(ng/m^3)	0.423	0.09	0.164	0.164	0.081
IP	(ng/m^3)	1.043	0.208	0.375	0.375	0.224
TOTAL	(ng/m^3)	5.933	1.493	2.635	2.635	1.948

Note. In addition, analyses of the samples before and after intense dust event are given.

4. Conclusions

In this study, the coupled meteorological and air quality WRF-Chem model was used to simulate the severe dust storm that occurred over southeastern Europe from 27 to 30 March 2020. Modeled hourly PM_{10} concentrations were compared with hourly values observed at several air quality stations in Croatia. In addition, a qualitative assessment of the modeled AOD was performed using AERONET observations and MERRA-2 products. Independently, the chemical and SEM morphological analyzes of PM_{10} samples collected at the Teaching Institute of Public Health (the TIPH station) in Rijeka on the northeastern Adriatic coast were performed.

The unprecedented increase in airborne particulate matter during the dust outbreak took place in the Balkan region. On 27 March 2020, the daily PM_{10} value observed at the TIPH station was ∼7.7 times higher than the average value in 2020. The remote sensing and modeling results showed the influence of two different sources. The contribution from North Africa was in the middle troposphere. It appeared the day before the peak of observed PM_{10} levels, which according to the modeling results may be caused by advection up to ∼2 km above sea level from the sources east of the Caspian Sea. The modeling results showed a high correlation with hourly PM_{10} levels observed at several air quality stations in Croatia but underestimated the observations by 26%–57% on average. According to AERONET measurements at Lampedusa and Galata stations, the plume from Asian sources was underestimated more. The HYSPLIT back trajectories indicate that the source is located in the dried Aral Sea. The erodibility map based on the simple source function in WRF proves inadequate for the smaller desert areas. In this case, the erodibility values over the Aral Sea are zero, and this is the most likely reason for most of the existing biases in PM_{10} and AOD. On the other hand, the analyses of trace metals and SEM of PM_{10} collected over the northern Adriatic Sea during the most intense dust event in March 2020 suggest that the PM_{10} filter mainly reflects the influence of Saharan dust.

Although it can be argued with high probability that both sources of dust particles, that is, the Aral and the Saharan regions, contributed to the development of this extreme event, it is difficult to estimate their contribution to PM_{10} concentrations at air quality stations in Croatia. While the modeling and remote sensing results (qualitative) support the conclusion that the Asian sources and especially the Aral desert region contribute significantly to the increase in PM_{10} concentration, the chemical and SEM results have shown that a certain part of the dust originates from the Sahara. The arguments in favor of Asian sources being the most significant: the increased AOD identifying plumes from both the Sahara and Asia, but the advection from the east occurred in the lower troposphere and the atmospheric boundary layer, while the African plume was in the middle troposphere above the mixed layer. It is important to emphasize that Mediterranean cyclones may facilitate the long-range transport of giant mineral dust particles (>75 μm, Flaounas et al., 2022). Thus, if the coarser particles can be uplifted and transported to distant regions, the deposition by gravitational settling may be the main mechanism to explain the presence of Saharan dust in the filter. The trajectory of the cyclone combined with the subsidence within anticyclonic conditions further favors the formation of dusty air of Saharan origin on the filters.

The analysis of this extreme event also contributes to a better knowledge of the atmospheric dynamics related to climate change, since there are some predictions about the potential expansion of desert areas due to the increase in temperature and the possible decrease in precipitation in the subtropics. Thus, one possible scenario is that intense dust transport events could become more frequent in Europe, and therefore it is important to emphasize the need for further investigation of such events.

10.1029/2023EA002879

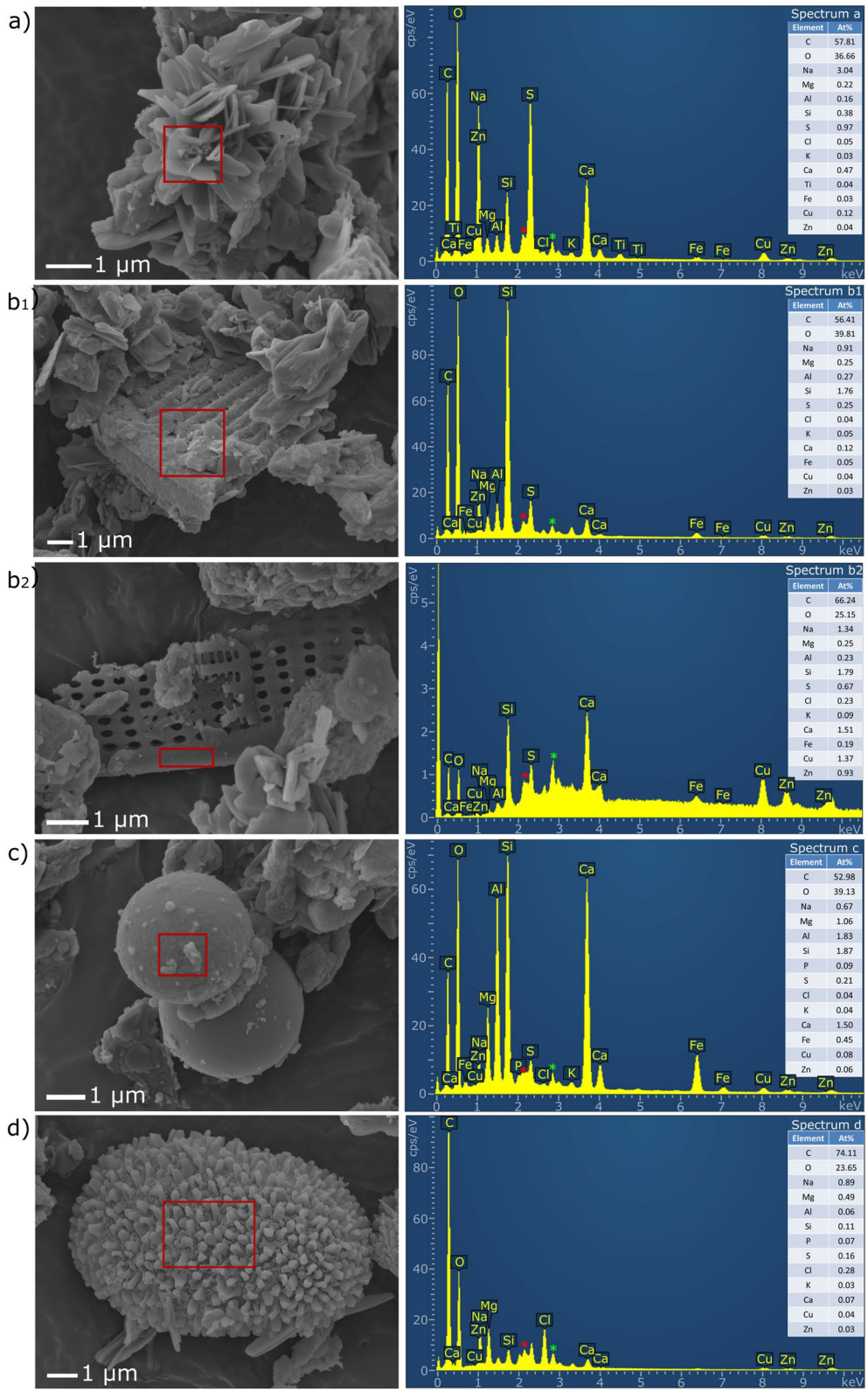

Figure 9. Representative scanning electron microscope (SEM) images (including corresponding energy dispersive X-ray spectrometer (EDS) spectra observed from positions marked by red frames in the SEM images) of GFF filter bearing PM_{10} collected during the intense dust event in March 2020 showing: (a) glauberite $Na_2Ca(SO_4)_2$ and/or $CaSO_4 \times 2H_2O$ desert rose gypsum typical of North Africa; (b1/b2) fragments of diatom skeletons mixed with dust; (c) aluminosilicates with embedded Fe; (d) primary biological aerosol particles (PBAPs), as also found in Barkley et al. (2021). In the spectra of EDS, the asterisks represent the peaks originating from the coating material: red for Au and green for Pd.

Data Availability Statement

The boundary conditions for WRF-Chem were obtained from ECMWF data sets at https://www.ecmwf.int/en/forecasts/access-forecasts/access-archive-datasets. MERRA-2 data were downloaded at the Modeling and Assimilation Data and Information Services (MDISC) at https://gmao.gsfc.nasa.gov/reanalysis/MERRA-2/data_access/ managed by the NASA Goddard Earth Sciences (GES) Data and Information Center (DISC) (GMAO, 2015a, 2015b). The AOD data by MODIS were obtained at: https://ladsweb.modaps.eosdis.nasa.gov/missions-and-measurements/products/MYD04_L2. The AOD observations from the AERONET network were taken from https://aeronet.gsfc.nasa.gov/ (Holben et al., 1998). The authors gratefully acknowledge the NOAA Air Resources Laboratory (ARL) for the provision of the HYSPLIT transport and dispersion model and/or READY website (https://www.ready.noaa.gov) used in this publication (Stein et al., 2015). The sampling and chemical analysis of the PM_{10} was made by the Teaching Institute of Public Health, Rijeka, while SEM analyses were performed at the Faculty of Physics, University of Rijeka. For most of the figures, the NCL software was used (NCAR Command Language, 2019).

Acknowledgments

The authors gratefully acknowledge support from Croatian Science Foundation project IP-2018-01-1717-MARRES for initiating the research, chemical analyses, and interpretation of data, and discussion. We thank the Faculty of Natural Sciences of the University of Zagreb and the University of Rijeka, project uniri-prirod-18-232 for financial support. Our thanks go to Prof. Dr. P. Orlović-Leko for the productive discussion on the dust event; Prof. Dr. D. Viličić and Dr. S. Bosak for help in the interpretation of SEM results related to biological material.

References

Alebić-Juretić, A. (2015). Airborne polycyclic aromatic hydrocarbons in suspended particulates from the urban atmosphere of Rijeka, Croatia. *Polycyclic Aromatic Compounds*, *35*(1), 91–101. https://doi.org/10.1080/10406638.2014.922106

Alpert, P., & Ziv, B. (1989). The Sharav Cyclone: Observations and some theoretical considerations. *Journal of Geophysical Research*, *94*(D15), 18495. https://doi.org/10.1029/jd094id15p18495

Barkley, A. P., Olson, N. E., Prospero, J. M., Gatineau, A., Panechou, K., Maynard, N. G., et al. (2021). Atmospheric transport of North African dust-bearing supermicron freshwater diatoms to South America: Implications for iron transport to the equatorial North Atlantic Ocean. *Geophysical Research Letters*, *48*(5). https://doi.org/10.1029/2020GL090476

Barnaba, F., & Gobbi, G. P. (2004). Aerosol seasonal variability over the Mediterranean region and relative impact of maritime, continental and Saharan dust particles over the basin from MODIS data in the year 2001. *Atmospheric Chemistry and Physics*, *4*(9/10), 2367–2391. https://doi.org/10.5194/acp-4-2367-2004

Benedetti, A., Baldasano, J. M., Basart, S., Benincasa, F., Boucher, O., Brooks, M. E., et al. (2014). Operational dust prediction. In P. Knippertz & J. B. Stuut (Eds.), *Mineral dust*. Springer. https://doi.org/10.1007/978-94-017-8978-3_10

Buchard, V., Randles, C. A., da Silva, A., Darmenov, A. S., Colarco, P. R., Govindaraju, R. C., et al. (2017). The MERRA-2 aerosol reanalysis, 1980-onward, Part II: Evaluation and case studies. *Journal of Climate*, *30*(17), 6851–6872. https://doi.org/10.1175/jcli-d-16-0613.1

Chen, F., & Dudhia, J. (2001). Coupling an advanced land surface-hydrology model with Penn State-NCAR MM5 modeling system. Part I: Model implementation and sensitivity. *Monthly Weather Review*, *129*(4), 569–585. https://doi.org/10.1175/1520-0493(2001)129<0569:CAALSH>2.0.CO;2

Chin, M., Rood, R. B., Lin, S.-J., Müller, J.-F., & Thompson, A. (2000). Atmospheric sulfur cycle simulated in the global model GOC.4RT: Model description and global properties. *Journal of Geophysical Research*, *105*(D20), 24671–24687. https://doi.org/10.1029/2000jd900384

Choobari, O. A., Zawar-Reza, P., & Sturman, A. (2012). Feedback between wind-blown dust and planetary boundary-layer characteristics: Sensitivity to boundary and surface layer parameterizations. *Atmospheric Environment*, *61*, 294–304. https://doi.org/10.1016/j.at-mosenv.2012.07.038

Colarco, P., da Silva, A., Chin, M., & Diehl, T. (2010). Online simulations of global aerosol distributions in the NASA GEOS-4 model and comparisons to satellite and ground-based aerosol optical depth. *Journal of Geophysical Research*, *115*(D14), D14207. https://doi.org/10.1029/2009jd012820

Cremades, P. G., Fernández, R. P., Allende, D. G., Mulena, G. C., & Puliafito, S. E. (2016). High resolution satellite derived erodibility factors for WRF/Chem windblown dust simulations in Argentina. *Atmósfera*, *30*(1), 11–25. https://doi.org/10.20937/ATM.2017.30.01.02

Engelstaedter, S., Tegen, I., & Washington, R. (2006). North African dust emissions and transport. *Earth-Science Reviews*, *79*(1–2), 73–100. https://doi.org/10.1016/j.earscirev.2006.06.004

European Centre for Medium-Range Weather Forecasts (ECMWF). (2020). Boundary conditions [Dataset]. Retrieved from https://www.ecmwf.int/en/forecasts/access-forecasts/access-archive-datasets

Federici, E., Petroselli, C., Montalbani, E., Casagrande, C., Ceci, E., Moroni, B., et al. (2018). Airborne bacteria and persistent organic pollutants associated with an intense Saharan dust event in the Central Mediterranean. *Science of the Total Environment*, *645*(15), 401–410. https://doi.org/10.1016/j.scitotenv.2018.07.128

Fiedler, S., Schepanski, K., Knippertz, P., Heinold, B., & Tegen, I. (2014). How important are atmospheric depressions and mobile cyclones for emitting mineral dust aerosol in North Africa? *Atmospheric Chemistry and Physics*, *14*(17), 8983–9000. https://doi.org/10.5194/acp-14-8983-2014

Flaounas, E., Davolio, S., Raveh-Rubin, S., Pantillon, F., Miglietta, M. M., Gaertner, M. A., et al. (2022). Mediterranean cyclones: Current knowledge and open questions on dynamics, prediction, climatology and impacts. *Weather and Climate Dynamics*, *3*(1), 173–208. https://doi.org/10.5194/wcd-3-173-2022

Gašparac, G., Jeričević, A., Kumar, P., & Grisogono, B. (2020). Regional-scale modelling for the assessment of atmospheric particulate matter concentrations at rural background locations in Europe. *Atmospheric Chemistry and Physics*, *20*(11), 6395–6415. https://doi.org/10.5194/acp-20-6395-2020

Ge, Y., Abuduwaili, J., Ma, L., & Liu, D. (2016). Temporal variability and potential diffusion characteristics of dust aerosol originating from the Aral Sea basin, Central Asia. *Water, Air, and Soil Pollution*, *227*(2), 63. https://doi.org/10.1007/s11270-016-2758-6

Gillette, D. A., & Passi, R. (1988). Modeling dust emission caused by wind erosion. *Journal of Geophysical Research*, *93*(D11), 14233–14242. https://doi.org/10.1029/JD093iD11p14233

Ginoux, P., Chin, M., Tegen, I., Prospero, J. M., Holben, B., Dubovik, O., & Lin, S. J. (2001). Sources and distributions of dust aerosols simulated with the GOCART model. *Journal of Geophysical Research*, *106*(D17), 20255–20273. https://doi.org/10.1029/2000JD000053

Global Modeling and Assimilation Office (GMAO). (2015a). MERRA-2 tavg1_2d_aer_Nx: 2d,1-hourly, time-averaged, single-level, assimilation, aerosol diagnostics V5.12.4 [Dataset]. Goddard Earth Sciences Data and Information Services Center (GES DISC). https://doi.org/10.5067/KLICLTZ8EM9D

Global Modeling and Assimilation Office (GMAO). (2015b). MERRA-2 tavg1_2d_slv_Nx: 2d,1-hourly, time-averaged, single-level, assimilation, single-level diagnostics V5.12.4 [Dataset]. Goddard Earth Sciences Data and Information Services Center (GES DISC). https://doi.org/10.5067/VJAFPLI1CSIV

Goudie, A. S., & Middleton, N. J. (2006). *Desert dust in the global system*. Springer.

Grell, G. A., Peckham, S. E., Schmitz, R., McKeen, S. A., Frost, G., Skamarock, W. C., & Eder, B. (2005). Fully coupled "online" chemistry within the WRF model. *Atmospheric Environment*, *39*(37), 6957–6975. https://doi.org/10.1016/j.atmosenv.2005.04.027

Groll, M., Opp, C., Issanova, G., Vereshagina, N., & Semenov, O. (2019). Physical and chemical characterization of dust deposited in the Turan lowland (Central Asia). *Proc. E3S Web Conf.*, *99*, 03005.

Heinold, B., Knippertz, P., Marsham, J. H., Fiedler, S., Dixon, N. S., Schepanski, K., et al. (2013). The role of deep convection and nocturnal low-level jets for dust emission in summertime West Africa: Estimates from convection-permitting simulations. *Journal of Geophysical Research: Atmospheres*, *118*(10), 4385–4400. https://doi.org/10.1002/jgrd.50402

Holben, B. N., Eck, T. F., Slutsker, I., Tanre, D., Buis, J. P., Stezer, A., et al. (1998). AERONET-A federated instrument network and data archive for aerosol characterization [Dataset]. Remote Sensing of Environment, *66*, 1–16. https://doi.org/10.1016/s0034-4257(98)00031-5

Hsu, N. C., Tsay, S. C., King, M. D., & Herman, J. R. (2004). Aerosol properties over bright-reflecting source regions. *IEEE Transactions on Geoscience and Remote Sensing*, *42*(3), 557–569. https://doi.org/10.1109/TGRS.2004.824067

Huneeus, N., Schulz, M., Balkanski, Y., Griesfeller, J., Prospero, J., Kinne, S., et al. (2011). Global dust model intercomparison in AeroCom phase I. *Atmospheric Chemistry and Physics*, *11*(15), 7781–7816. https://doi.org/10.5194/acp-11-7781-2011

Iacono, M. J., Delamere, J. S., Mlawer, E. J., Shephard, M. W., Clough, S. A., & Collins, W. D. (2008). Radiative forcing by long-lived greenhouse gases: Calculations with the AER radiative transfer models. *Journal of Geophysical Research*, *113*(D13), D13103. https://doi.org/10.1029/2008jd009944

Indoitu, R., Orlovsky, L., & Orlovsky, N. (2012). Dust storms in central Asia: Spatial and temporal variations. *Journal of Arid Environment*, *85*, 62–70. https://doi.org/10.1016/j.jaridenv.2012.03.018

Israelevich, P., Ganor, E., Alpert, P., Kishcha, P., & Stupp, A. (2012). Predominant transport paths of Saharan dust over the Mediterranean Sea to Europe. *Journal of Geophysical Research*, *117*(D2), D02205. https://doi.org/10.1029/2011JD016482

Karami, S., Hamzeh, N. H., Kaskaoutis, D. G., Rashki, A., Alam, K., & Ranjbar, A. (2021). Numerical simulations of dust storms originated from dried lakes in central and southwest Asia: The case of Aral Sea and Sistan Basin. *Aeolian Research*, *50*, 100679. https://doi.org/10.1016/j.aeolia.2021.100679

Kaufman, Y. J., Tanré, D., Remer, L., Vermote, E., Chu, A., & Holben, B. N. (1997). Remote sensing of tropospheric aerosol from EOS-MODIS over the land using dark targets and dynamic aerosol models. *Journal of Geophysical Research*, *102*(D14), 17051–17067. https://doi.org/10.1029/96JD03988

Kehler-Poljak, G., Telišman Prtenjak, M., Kvakić, M., Šariri, K., & Večenaj, Ž. (2017). Interaction of sea breeze and deep convection over the Northeastern Adriatic Coast: An analysis of sensitivity experiments using a high-resolution mesoscale model. *Pure and Applied Geophysics*, *174*(11), 4197–4224. https://doi.org/10.1007/s00024-017-1607-x

Kleist, D. T., Parrish, D. F., Derber, J. C., Treadon, R., Wu, W.-S., & Lord, S. (2009). Introduction of the GSI into the NCEP global data assimilation system. *Weather and Forecasting*, *24*(6), 1691–1705. https://doi.org/10.1175/2009waf2222201.1

Kok, J. F., Adebiyi, A. A., Albani, S., Balkanski, Y., Checa-Garcia, R., Chin, M., et al. (2021a). Improved representation of the global dust cycle using observational constraints on dust properties and abundance. *Atmospheric Chemistry and Physics*, *21*(10), 8127–8167. https://doi.org/10.5194/acp-21-8127-2021

Kok, J. F., Adebiyi, A. A., Albani, S., Balkanski, Y., Checa-Garcia, R., Chin, M., et al. (2021b). Contribution of the world's main dust source regions to the global cycle of desert dust. *Atmospheric Chemistry and Physics*, *21*(10), 8169–8193. https://doi.org/10.5194/acp-21-8169-2021

Kumar, R., Barth, M. C., Pfister, G. G., Naja, M., & Brasseur, G. P. (2014). WRF-chem simulations of a typical pre-monsoon dust storm in northern India: Influences on aerosol optical properties and radiation budget. *Atmospheric Chemistry and Physics*, *14*(5), 2431–2446. https://doi.org/10.5194/acp-14-2431-2014

Kylander, M. E., Martínez-Cortizas, A., Bindler, R., Kaal, J., Sjöström, J. K., Hansson, S. V., et al. (2018). Mineral dust as a driver of carbon accumulation in northern latitudes. *Scientific Reports*, *8*(1), 6876. https://doi.org/10.1038/s41598-018-25162-9

LeGrand, S. L., Polashenski, C., Letcher, T. W., Creighton, G. A., Peckham, S. E., & Cetola, J. D. (2019). The AFWA dust emission scheme for the GOCART aerosol model in WRF-Chem v3.8.1. *Geoscientific Model Development*, *12*(1), 131–166. https://doi.org/10.5194/gmd-12-131-2019

Levy, R., Hsu, C., et al. (2015). MODIS atmosphere L2 aerosol product [Dataset]. NASA MODIS Adaptive Processing System, Goddard Space Flight Center, USA. http://dx.doi.org/10.5067/MODIS/MOD04_L2.006

Li, L., & Sokolik, I. N. (2018). The dust direct radiative impact and its sensitivity to the land surface state and key minerals in the WRF-chem-DuMo model: A case study of dust storms in central Asia. *Journal of Geophysical Research: Atmospheres*, *123*(9), 4564–4582. https://doi.org/10.1029/2017JD027667

Lo, J. C.-F., Yang, Z.-L., & Pielke, R. A., Sr. (2008). Assessment of three dynamical climate downscaling methods using the Weather Research and Forecasting (WRF) model. *Journal of Geophysical Research*, *113*(D9), D09112. https://doi.org/10.1029/2007JD009216

Micklin, P. (2007). The Aral Sea disaster. *Annual Review of Earth and Planetary Sciences*, *35*(1), 47–72. https://doi.org/10.1146/annurev.earth.35.031306.140120

Mifka, B., Telišman Prtenjak, M., Kavre Piltaver, I., Mekterović, D., Kuzmić, J., Marcijuš, M., & Ciglenečki, I. (2022a). The aspects of numerical simulations on desert dust outbreaks over the Adriatic Sea; influence of Asian and African deserts. In S. Trini-Castelli, A. I. Miranda, B. Augusto, & J. Ferreira (Eds.), *HARMO 21, proceedings of the 21st international conference on harmonisation within atmospheric dispersion modelling for regulatory purposes* (pp. 129–130). Universidade de Aveiro.

Mifka, B., Telišman Prtenjak, M., Kuzmić, J., Čanković, M., Mateša, S., & Ciglenečki, I. (2022b). Climatology of dust deposition in the Adriatic Sea; a possible impact on marine production. *Journal of Geophysical Research: Atmospheres*, *127*(7), e2021JD035783. https://doi.org/10.1029/2021JD035783

Mifka, B., Žurga, P., Kontošić, D., Odorčić, D., Mezlar, M., Merico, E., et al. (2021). Characterization of airborne particulate fractions from the port city of Rijeka, Croatia. *Marine Pollution Bulletin*, *166*, 112–236. https://doi.org/10.1016/j.marpolbul.2021.112236

Molod, A., Takacs, L., Suarez, M., & Bacmeister, J. (2015). Development of the GEOS-5 atmospheric general circulation model: Evolution from MERRA to MERRA2. *Geoscientific Model Development*, *8*(5), 1339–1356. https://doi.org/10.5194/gmd-8-1339-2015

Morrison, H., Curry, J. A., & Khvorostyanov, V. I. (2005). A new double-moment microphysics parameterization for application in cloud and climate models, Part I: Description. *Journal of the Atmospheric Sciences*, *62*(6), 1665–1677. https://doi.org/10.1175/jas3446.1

Moulin, C., Lambert, C. E., Dayan, U., Masson, V., Ramonet, M., Bousquet, P., et al. (1998). Satellite climatology of African dust transport in the Mediterranean atmosphere. *Journal of Geophysical Research*, *103*(111), 13137–13144. https://doi.org/10.1029/98JD00171

Nakanishi, M., & Niino, H. (2009). Development of an improved turbulence closure model for the atmospheric boundary layer. *Journal of the Meteorological Society of Japan*, *87*(5), 895–912. https://doi.org/10.2151/jmsj.87.895
NCAR Command Language. (2019). NCAR Command Language (version 6.6.2) [Software]. UCAR/NCAR/CISL/TDD. https://doi.org/10.5065/D6WD3XH5
O'Hara, S. L., Wiggs, G. F., Mamedov, B., Davidson, G., & Hubbard, R. B. (2000). Exposure to airborne dust contaminated with pesticide in the Aral Sea region. *The Lance*, *355*(9204), 627–628. https://doi.org/10.1016/s0140-6736(99)04753-4
Palacios-Peña, L., Lorente-Plazas, R., Montávez, J. P., & Jiménez-Guerrero, P. (2019). Saharan dust modeling over the Mediterranean Basin and Central Europe: Does the resolution matter? *Frontiers of Earth Science*, *7*, 290. https://doi.org/10.3389/feart.2019.00290
Pantillon, F., Knippertz, P., Marsham, J. H., Panitz, H.-J., & Bischoff-Gauss, I. (2016). Modeling haboob dust storms in large-scale weather and climate models. *Journal of Geophysical Research: Atmospheres*, *121*(5), 2090–2109. https://doi.org/10.1002/2015JD024349
Pielke, R. A., & Mahrer, Y. (1978). Verification analysis of the University of Virginia three-dimensional mesoscale model prediction over South Florida for July 1, 1973. *Monthly Weather Review*, *106*(11), 1568–1589. https://doi.org/10.1175/1520-0493(1978)106<1568:vaotuo>2.0.co;2
Reichle, R. H., Liu, Q., Koster, R. D., Draper, C. S., Mahanama, S. P. P., & Partyka, G. S. (2017). Land surface precipitation in MERRA-2. *Journal of Climate*, *30*(5), 1643–1664. https://doi.org/10.1175/JCLI-D-16-0570.1
Richon, C., Dutay, J.-C., Dulac, F., Wang, R., & Balkanski, Y. (2018). Modeling the biogeochemical impact of atmospheric phosphate deposition from desert dust and combustion sources to the Mediterranean Sea. *Biogeosciences*, *15*(8), 2499–2524. https://doi.org/10.5194/bg-15-2499-2018
Ridley, D. A., Heald, C. L., Kok, J. F., & Zhao, C. (2016). An observationally constrained estimate of global dust aerosol optical depth. *Atmospheric Chemistry and Physics*, *16*(23), 15097–15117. https://doi.org/10.5194/acp-16-15097-2016
Rizza, U., Barnaba, F., Miglietta, M. M., Mangia, C., Di Liberto, L., Dionisi, D., et al. (2017). WRF-Chem model simulations of a dust outbreak over the central Mediterranean and comparison with multi-sensor desert dust observations. *Atmospheric Chemistry and Physics*, *17*(1), 93–115. https://doi.org/10.5194/acp-17-93-2017
Romagnoli, P., Balducci, C., Perilli, M., Perreca, E., & Cecinato, A. (2016). Particulate PAHs and n-alkanes in the air over southern and eastern Mediterranean Sea. *Chemosphere*, *159*, 516–552. https://doi.org/10.1016/j.chemosphere.2016.06.024
Roy, S. B., Smith, M., Morris, L., Orlovsky, N., & Khalilov, A. (2014). Impact of the desiccation of the Aral Sea on summertime surface air temperatures. *Journal of Arid Environments*, *110*, 79–85. https://doi.org/10.1016/j.jaridenv.2014.06.008
Sardoo, S. F., Mesbahzadeh, T., Salajeghe, A., Zehtabian, G., Ranjbar, A., Miglietta, M. M., & Krakauer, N. (2022). Antecedent soil moisture conditions influenced vertical dust flux: A case study in Iran using WRF-chem model. *Land*, *11*(6), 819. https://doi.org/10.3390/land11060819
Schepanski, K., Mallet, M., Heinold, B., & Ulrich, M. (2016). North African dust transport toward the western Mediterranean Basin: Atmospheric controls on dust source activation and transport pathways during June-July 2013. *Atmospheric Chemistry and Physics*, *16*(22), 14147–14168. https://doi.org/10.5194/acp-16-14147-2016
Schepanski, K., Tegen, I., & Macke, A. (2012). Comparison of satellite based observations of Saharan dust source areas. *Remote Sensing of Environment*, *123*, 90–97. https://doi.org/10.1016/j.rse.2012.03.019
Shao, Y., Wyrwoll, K.-H., Chappell, A., Huang, J., Lin, Z., McTainsh, G. H., et al. (2011). Dust cycle: An emerging core theme in Earth system science. *Aeolian Research*, *2*(4), 181–204. https://doi.org/10.1016/j.aeolia.2011.02.001
Sharma, A., Huang, H. P., Zavialov, P., & Khan, V. (2018). Impact of desiccation of Aral Sea on the regional climate of Central Asia using WRF model. *Pure and Applied Geophysics*, *175*(1), 465–478. https://doi.org/10.1007/s00024-017-1675-y
Skamarock, W. C., Klemp, J. B., Dudhia, J., Gill, D. O., Barker, D. M., Wang, W., & Powers, J. G. (2008). *A description of the advanced research WRF version 2*. NCAR technical note, NCAR/TN-468+STR. National Center for Atmospheric Research. Retrieved from http://wrf-model.org/wrfadmin/publications.php
Skamarock, W. C., Klemp, J. B., Dudhia, J., Gill, D. O., Liu, Z., Berner, J., et al. (2019). A description of the advanced research WRF model version 4.1 (No. NCAR/TN-556+STR). Undefined. https://doi.org/10.5065/1dfh-6p97
Stein, A. F., Draxler, R. R., Rolph, G. D., Stunder, B. J. B., Cohen, M. D., & Ngan, F. (2015). NOAA's HYSPLIT atmospheric transport and dispersion modeling system [Software]. Bulletin of the American Meteorological Society, *96*(12), 2059–2077. https://doi.org/10.1175/bams-d-14-00110.1
Strelec Mahović, N., Prieto, J., Jeričević, A., Gasparac, G., & Smiljanić, I. (2020). EUMETSAT webpage. Retrieved from https://www.eumetsat.int/aralkum-desert-dust-pollutes-air-south-east-europe
Teixeira, J. C., Carvalho, A. C., Carvalho, M. J., Luna, T., & Rocha, A. (2014). Sensitivity of the WRF model to the lower boundary in an extreme precipitation event—Madeira island case study. *Natural Hazards and Earth System Sciences*, *14*(8), 2009–2025. https://doi.org/10.5194/nhess-14-2009-2014
Teixeira, J. C., Carvalho, A. C., Tuccella, P., Curci, G., & Rocha, A. (2016). WRF-chem sensitivity to vertical resolution during a saharan dust event. *Physics and Chemistry of the Earth, Parts A/B/C*, *94*, 188–195. https://doi.org/10.1016/j.pce.2015.04.002
Tositti, L., Brattich, E., Cassardo, C., Morozzi, P., Bracci, A., Marinoni, A., et al. (2022). Development and evolution of an anomalous Asian dust event across Europe in March 2020. *Atmospheric Chemistry and Physics*, *22*(6), 4047–4073. https://doi.org/10.5194/acp-22-4047-2022
Tsarpalis, K., Katsafados, P., Papadopoulos, A., & Mihalopoulos, N. (2020). Assessing desert dust indirect effects on cloud microphysics through a cloud nucleation scheme: A case study over the Western Mediterranean. *Remote Sensing*, *12*(21), 3473. https://doi.org/10.3390/rs12213473
Varga, G. (2020). Changing nature of Saharan dust deposition in the Carpathian Basin (Central Europe): 40 years of identified North African dust events (1979–2018). *Environment International*, *139*, 105712. https://doi.org/10.1016/j.envint.2020.105712
Vincent, J., Laurent, B., Losno, R., Bon Nguyen, E., Roullet, P., Sauvage, S., et al. (2016). Variability of mineral dust deposition in the western Mediterranean Basin and South-East of France. *Atmospheric Chemistry and Physics*, *16*(14), 8749–8766. https://doi.org/10.5194/acp-16-8749-2016
Wæhler, T. A., & Dietrichs, E. S. (2017). The vanishing Aral Sea: Health consequences of an environmental disaster. *Tidsskr Nor Legeforen*. https://doi.org/10.4045/tidsskr.17.0597
Whish-Wilson, P. (2002). The Aral Sea environmental health crisis. *Journal of Rural and Remote Environmental Health*, *1*, 29–34.
Wu, C., Lin, Z., & Liu, X. (2020). The global dust cycle and uncertainty in CMIP5 (Coupled Model Intercomparison Project phase 5) models. *Atmospheric Chemistry and Physics*, *20*(17), 10401–10425. https://doi.org/10.5194/acp-20-10401-2020